IMA Journal of Applied Mathematics (2006) **71**, 715–739
doi:10.1093/imamat/hxh116
Advance Access publication on February 20, 2006

Long-wave linear stability theory for two-fluid channel flow including compressibility effects

TETYANA M. SEGIN
Department of Chemical and Materials Engineering, University of Alberta, Edmonton, Alberta, Canada T6G 2G6

LOU KONDIC†
Department of Mathematical Sciences, Center for Applied Mathematics and Statistics, New Jersey Institute of Technology, Newark, NJ 07102, USA

AND

BURT S. TILLEY
Franklin W. Olin College of Engineering, Needham, MA 02492, USA

[Received on 23 May 2005; accepted on 10 January 2006]

We present the linear stability of the laminar flow of an immiscible system of a compressible gas and incompressible liquid separated by an interface with large surface tension in a thin inclined channel. The flow is driven by an applied pressure drop and gravity. Following the air–water case, which is found in a variety of engineering systems, the ratio of the characteristic values of the gas and liquid densities and viscosities are assumed to be disparate. Under the lubrication approximation, and assuming ideal gas behaviour and isothermal conditions, this approach leads to a coupled non-linear system of partial differential equations describing the evolution of the interface between the gas and the liquid and the streamwise density distribution of the gas. This system also includes the effects of viscosity stratification, inertia, shear and capillarity. A linear stability analysis that allows for physically relevant non-zero pressure-drop base state is then performed. In contrast to the zero-pressure drop case which is amenable to the classical normal-mode approach, this configuration requires numerically solving a boundary-value problem for the gas density and interfacial deviations from the base state in the streamwise coordinate. We find that the effect of the gas compressibility on the interfacial stability in the limit of vanishingly small wavenumber is destabilizing, even for Stokes flow in the liquid. However, for finite wavenumber disturbances, compressibility may have stabilizing effects. In this regime, sufficient shear is required to destabilize the flow.

Keywords: two-fluid flow; compressibility.

1. Introduction

Liquid films are encountered in many physical situations. Examples of their practical application include oil and gas flows (see Oddie & Pearson, 2004, for recent review), a variety of cooling applications (see, e.g. Mudawar, 2001; Qu & Mudawar, 2003), in particular related to on-chip cooling of micro-electromechanical devices (Pettigrew *et al.*, 2001; Trebotich *et al.*, 2001; Kirshberg *et al.*, 2000). Two-phase gas–liquid flows are also important in a number of space-related operations including the

†Email: kondic@oak.njit.edu

design and operation of spacecraft environmental systems (Zhang *et al.*, 2002), the storage and transfer of cryogenic fluids and safety and performance issues related to space-based nuclear power systems (Dukler *et al.*, 1988; Bousman *et al.*, 1996). Knowledge about the physical properties of fluids and their effects on flow characteristics is important to understand the fundamental nature of two-phase flow.

Most of the existing theoretical works on two-fluid flows neglect compressibility of both fluids, even if one of them is a gas. Often, this approximation is motivated by the fact that the Mach number may be small in these flows. However, compressibility 'cannot' be neglected in flows of gases through narrow channels even if the Mach number is small (Faber, 2001). In these flows, an appreciable pressure difference may exist between the inlet and outlet regions, resulting in appreciable density changes. This effect is particularly relevant for flows in microchannels (Mudawar, 2001; Qu & Mudawar, 2003).

There are several prior works devoted to weakly compressible flows. In this limit, Hagstrom & Lorenz (1998) find that the solution remains smooth for all times and, to the leading order, it consists of the corresponding incompressible flow plus a highly oscillatory part describing sound waves. Alexakis *et al.* (2002), motivated by an astrophysical problem (where mixing across material interfaces driven by shear flows may significantly affect the dynamical evolution) show in their linear stability analysis that compressibility decreases the growth rate of instability. Rusak & Lee (2004) investigate the influence of the compressibility on the appearance of instabilities and transition (breakdown) phenomena in a compressible inviscid axisymmetric and rotating columnar flow of perfect gas in a finite-length straight circular pipe. They report the stabilizing effect of compressibility on vortex flows. The results are not as clear in flows that are subject to Rayleigh–Taylor instability, where compressibility can have both stabilizing and destabilizing effects; see Livescu (2003) and the references therein.

Figure 1 shows the basic geometry of the flow considered in this work. The two fluids can flow either cocurrently (both fluids flow in the same direction) or countercurrently (fluids flow in the opposite directions). Various aspects of the transition from the countercurrent flow (shown in Fig. 1) to a cocurrent flow adverse to gravity, as the adverse pressure drop is increased is called 'flooding'. These complicated non-linear effects appear typically when the gas phase is turbulent. Flooding has been investigated extensively both phenomenologically (Chang, 1986; Demekhin *et al.*, 1989; Fowler & Lisseter, 1992) and experimentally (see Bankoff & Lee, 1986, and the references therein, Mouza *et al.*, 2003) but the criteria for onset of flooding and related interfacial instabilities are still open to question.

The main goal of the present paper is to explore a simpler setup where the flow of both phases is laminar, but the constraint of incompressibility is removed from the gas phase. Through this linear analysis of a laminar flow, we find that there are unstable modes that correspond to spatially localized deflections of the interface and the gas pressure field. Although this work cannot directly connect the evolution of the unstable modes to the flooding phenomenon, these linearly unstable solutions are needed in order to explore their non-linear evolution. Hence, we concentrate on the interfacial stability in countercurrent flows with the hope of better understanding the phenomenon of flooding, although turbulent effects are not considered.

The paper is organized as follows. In Section 2, we derive equations that govern the interfacial dynamics for the flow of incompressible liquid and compressible gas. Section 3 is devoted to linear stability analysis. For reference, we consider the incompressible limit in Section 3.1, and then concentrate on the compressible case. Here, we observe that the general boundary condition for the density equation (prescribed values of the gas density at each end of the channel) implies that in general, the basic density state depends on the downstream coordinate. A simpler case, where this dependence is absent, is considered in Section 3.2. In this case, we proceed with the normal-mode analysis to investigate the behaviour of both interfacial and density modes. In Section 3.3, we consider the dynamics of countercurrent two-fluid flow for the case when the prescribed density values are different, and the base state

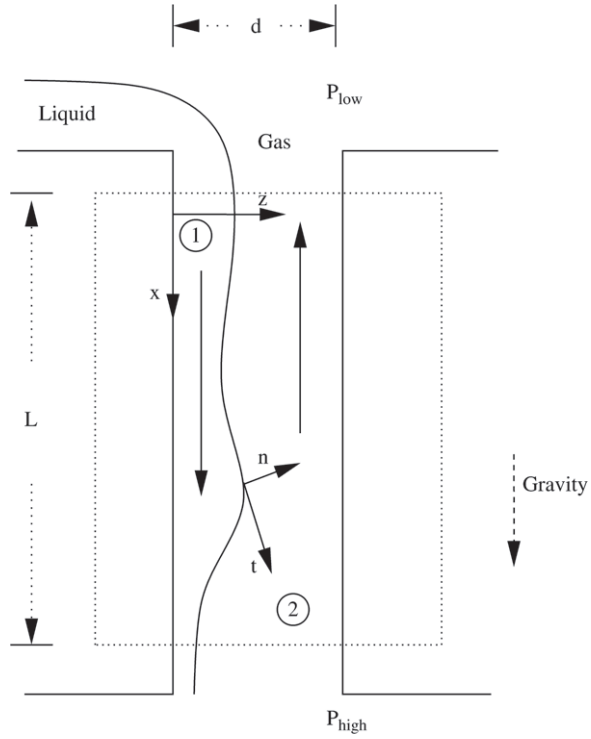

FIG. 1. Basic outline of the problem of interest. The plate on the left is coated by a liquid driven by gravity (pointing down), while the gas is driven by an adverse pressure drop (higher pressure at the bottom). This system can undergo hydrodynamic instabilities for sufficiently large adverse pressure drops. We consider only the domain in the dashed box in this work, and do not include the entrance or exit effects in the liquid or the gas. The local coordinate frame, based on the channel, is also shown. We note that most of the discussion concentrates on the vertical channel; however, the derivation of appropriate equations will be performed for the arbitrary angle of inclination.

is space dependent. In Section 4, we discuss the effect of compressibility on the interface stability in all considered configurations.

2. Formulation of equations

Consider the flow of two viscous fluids in a channel of height d and length L (Fig. 1) under isothermal conditions, where $\mathbf{n}$ is the unit normal pointing from the incompressible phase 1 (liquid) into the compressible phase 2 (gas) and $\mathbf{t}$ is the unit tangent vector at the interface. The equations that govern this system are continuity, the Navier–Stokes equations and an equation of state for the gas (asterisks denote dimensional variables):

$$\bar{\nabla} \cdot \mathbf{u}^{*(1)} = 0,$$

$$\rho_1^* \left(\frac{\partial \mathbf{u}^{*(1)}}{\partial t^*} + \mathbf{u}^{*(1)} \cdot \bar{\nabla} \mathbf{u}^{*(1)} \right) = -\bar{\nabla} p^{*(1)} + \rho_1^* \mathbf{g} + \mu_1^* \bar{\nabla}^2 \mathbf{u}^{*(1)},$$

$$\rho_{2t^*}^* + \bar{\nabla} \cdot (\rho_2^* \mathbf{u}^{*(2)}) = 0,$$

$$\rho_2^*\left(\frac{\partial \mathbf{u}^{*(2)}}{\partial t^*}+\mathbf{u}^{*(2)}\cdot\bar{\nabla}\mathbf{u}^{*(2)}\right)=-\bar{\nabla}p^{*(2)}+\rho_2^*\mathbf{g}+\mu_2^*\left(\bar{\nabla}^2\mathbf{u}^{*(2)}+\frac{1}{3}\bar{\nabla}(\bar{\nabla}\cdot\mathbf{u}^{*(2)})\right),$$

$$p^{*(2)}=K^*\rho_2^*.$$

The superscripts (1) and (2) on the dependent velocity and pressure variables correspond to phase 1 and phase 2, respectively, with corresponding densities ρ_i^*, dynamical viscosities μ_i^* and pressures $p^{*(i)}$; $\mathbf{g}$ is the gravitational acceleration. The last equation in the system relates the pressure and the density of the ideal gas under isothermal conditions ($pV = n\mathrm{R}T$). $K^* = \mathrm{R}T^*/M$, where R is the universal gas constant, T^* is the ambient temperature and M is the molecular weight of the gas, which gives that $\rho_2^* = nM/V$, where n is the number of moles of gas in the layer and V is the volume of the gas. Note further that in this case, K^* also represents the square of the speed of sound in the gas layer. Generally, we carry out the derivation for the arbitrary value of the inclination angle β; the case $\beta = \pi/2$ is illustrated in Fig. 1.

The velocities $\mathbf{u}^{*(i)} = (u^{*(i)}, w^{*(i)})$ satisfy the usual no-slip and no-penetration boundary conditions on the channel walls: $\mathbf{u}^{*(1)} = 0$ on $z^* = 0$ and $\mathbf{u}^{*(2)} = 0$ on $z^* = d$, as well as the balance of normal stress, balance of tangential stress, continuity of normal and tangential components of velocity and kinematic condition at $z^* = h^*(x^*, t^*)$:

$$[\mathbf{n}\cdot\mathbf{T}^*\cdot\mathbf{n}]=\sigma^*\kappa^*, \tag{2.1}$$

$$[\mathbf{t}\cdot\mathbf{T}^*\cdot\mathbf{n}]=0, \tag{2.2}$$

$$[\mathbf{u}^*\cdot\mathbf{n}]=0, \tag{2.3}$$

$$[\mathbf{u}^*\cdot\mathbf{t}]=0, \tag{2.4}$$

$$h_{t^*}^*+u^*h_{x^*}^*-w^*=0, \tag{2.5}$$

where the jump $[f]$ of the quantity f across the interface is denoted by $[f] = f^{(2)} - f^{(1)}$; $\mathbf{T}^*$ denotes the stress tensor, σ^* is the surface tension between the two fluids and κ^* is twice the mean curvature of the interface, given by

$$\kappa^*=-h_{x^*x^*}^*(1+h_{x^*}^{*2})^{-3/2}.$$

We scale lengths by d, densities by ρ_1^* and velocities by d^2g/ν_1^* ($\nu_1^* = \mu_1^*/\rho_1^*$ is the kinematic viscosity of phase 1) and

$$t=t^*dg/\nu_1^*;\quad p^{(i)}=p^{*(i)}/\rho_1^*dg.$$

Thus, we obtain

$$\nabla\cdot\mathbf{u}^{(1)}=0, \tag{2.6}$$

$$\mathrm{Re_l}\left\{\frac{\partial \mathbf{u}^{(1)}}{\partial t}+\mathbf{u}^{(1)}\cdot\nabla\mathbf{u}^{(1)}\right\}=-\nabla p^{(1)}+\hat{\mathbf{g}}+\nabla^2\mathbf{u}^{(1)}, \tag{2.7}$$

$$\bar{\rho}_t+\nabla\cdot(\bar{\rho}\mathbf{u}^{(2)})=0, \tag{2.8}$$

$$\mathrm{Re_l}\bar{\rho}\left\{\frac{\partial \mathbf{u}^{(2)}}{\partial t}+\mathbf{u}^{(2)}\cdot\nabla\mathbf{u}^{(2)}\right\}=-\nabla p^{(2)}+\bar{\rho}\hat{\mathbf{g}}+\bar{\mu}\left\{\nabla^2\mathbf{u}^{(2)}+\frac{1}{3}\nabla[\nabla\cdot\mathbf{u}^{(2)}]\right\}, \tag{2.9}$$

$$p^{(2)}=K\bar{\rho}, \tag{2.10}$$

where $\bar{\rho} = \rho_2^*/\rho_1^*$ is the density ratio, $\bar{\mu} = \mu_2^*/\mu_1^*$ is the viscosity ratio, $K = K^*/dg$, $\mathrm{Re_l} = gd^3/\nu_1^{*2}$ is the Reynolds number of phase 1, $\hat{\mathbf{g}}$ is the unit vector in the direction of gravity and velocities are $\mathbf{u}^{(i)} = (u^{(i)}, w^{(i)})$.

The boundary conditions on the channel walls become: $\mathbf{u}^{(1)} = 0$ on $z = 0$ and $\mathbf{u}^{(2)} = 0$ on $z = 1$ (Fig. 1). The conditions (2.1)–(2.5) at $z = h(x, t)$ become

$$[\mathbf{n} \cdot \mathbf{T} \cdot \mathbf{n}] = \sigma\kappa, \tag{2.11}$$

$$[\mathbf{t} \cdot \mathbf{T} \cdot \mathbf{n}] = 0, \tag{2.12}$$

$$[\mathbf{u} \cdot \mathbf{n}] = 0, \tag{2.13}$$

$$[\mathbf{u} \cdot \mathbf{t}] = 0, \tag{2.14}$$

$$h_t + uh_x - w = 0, \tag{2.15}$$

where

$$\sigma = \frac{\sigma^*}{\rho_1^* d^2 g}.$$

We are interested in gas–liquid systems where the density and dynamic viscosity ratios are small, see Segin *et al.* (2004). Following the case of air–water (under standard conditions: $\rho_2^*/\rho_1^* = 8 \times 10^{-4}$, $\mu_2^*/\mu_1^* = 2 \times 10^{-2}$, Batchelor, 1967), we assume that $\bar{\rho} = \rho_2^*/\rho_1^*$ is of the order ε^2 and $\bar{\mu} = \mu_2^*/\mu_1^*$ is of the order ε, where ε is an aspect ratio of channel thickness to a characteristic channel length, i.e. $\bar{\rho} = \varepsilon^2\rho$, $\bar{\mu} = \varepsilon\mu$, and ρ, μ are O(1). This distinguished limit allows us to capture the dominant physical effects in this system, while simplifying the analysis considerably.

We note that the ratio of the liquid Reynolds number to the gas Reynolds number is given by

$$\frac{\mathrm{Re_l}}{\mathrm{Re_g}} = \frac{dU_\mathrm{l}/\nu_1^*}{dU_\mathrm{g}/\nu_2^*} = \frac{\nu_2^*}{\nu_1^*}\frac{U_\mathrm{l}}{U_\mathrm{g}} = \frac{1}{\varepsilon}\frac{U_\mathrm{l}}{U_\mathrm{g}},$$

where U_l is the characteristic velocity of the liquid and U_g is the characteristic velocity of the gas. Therefore, the tangential gas velocity scale is $\mathrm{O}(U_\mathrm{l}/\varepsilon)$ for $\mathrm{Re_g} = \mathrm{Re_l} = \mathrm{O}(1)$.

Next, we assume that all changes of the flow occur on a spatial scale that is much longer than the channel thickness. Therefore, we use scaled variables $\xi = \varepsilon x$ and $\zeta = z$. The kinematic boundary condition (2.15) then requires introducing a slow time scale $\tau = \varepsilon t$.

Our system of equations (2.6)–(2.9) in the long-wave limit can be written in component form as

$$\varepsilon u_\xi^{(1)} + w_\zeta^{(1)} = 0, \tag{2.16}$$

$$\mathrm{Re_l}\varepsilon\left[u_\tau^{(1)} + u^{(1)}u_\xi^{(1)} + \tfrac{1}{\varepsilon}w^{(1)}u_\zeta^{(1)}\right] = -\varepsilon p_\xi^{(1)} + \cos\beta + \varepsilon^2\left(u_{\xi\xi}^{(1)} + \tfrac{1}{\varepsilon^2}u_{\zeta\zeta}^{(1)}\right), \tag{2.17}$$

$$\mathrm{Re_l}\varepsilon\left[w_\tau^{(1)} + u^{(1)}w_\xi^{(1)} + \tfrac{1}{\varepsilon}w^{(1)}w_\zeta^{(1)}\right] = -p_\zeta^{(1)} + \sin\beta + \varepsilon^2\left(w_{\xi\xi}^{(1)} + \tfrac{1}{\varepsilon^2}w_{\zeta\zeta}^{(1)}\right), \tag{2.18}$$

$$\varepsilon\rho_\tau + \varepsilon(\rho u^{(2)})_\xi + (\rho w^{(2)})_\zeta = 0, \tag{2.19}$$

$$\mathrm{Re}_l\varepsilon^2\rho[\varepsilon u_\tau^{(2)} + \varepsilon u^{(2)}u_\xi^{(2)} + w^{(2)}u_\zeta^{(2)}]$$
$$= -\varepsilon p_\xi^{(2)} + \varepsilon^2\rho\cos\beta + \frac{\mu}{3}(4\varepsilon^3 u_{\xi\xi}^{(2)} + 3\varepsilon u_{\zeta\zeta}^{(2)} + \varepsilon^2 w_{\zeta\xi}^{(2)}), \tag{2.20}$$

$$\mathrm{Re}_l\varepsilon^2\rho[\varepsilon w_\tau^{(2)} + \varepsilon u^{(2)}w_\xi^{(2)} + w^{(2)}w_\zeta^{(2)}]$$
$$= -p_\zeta^{(2)} + \varepsilon^2\rho\sin\beta + \frac{\mu}{3}(4\varepsilon w_{\zeta\zeta}^{(2)} + 3\varepsilon^3 w_{\xi\xi}^{(2)} + \varepsilon^2 u_{\zeta\xi}^{(2)}). \tag{2.21}$$

We assume a perturbation expansion for u in ε:

$$u^{(1)}(\xi,\zeta,\tau) = u_0^{(1)}(\xi,\zeta,\tau) + \varepsilon u_1^{(1)}(\xi,\zeta,\tau) + \cdots,$$

and then from the continuity equation (2.16), it follows that

$$w^{(1)}(\xi,\zeta,\tau) = \varepsilon\{w_0^{(1)}(\xi,\zeta,\tau) + \varepsilon w_1^{(1)}(\xi,\zeta,\tau) + \cdots\}.$$

The gas velocities in the second fluid have an asymptotic expansion of the form:

$$u^{(2)}(\xi,\zeta,\tau) = \frac{1}{\varepsilon}\{u_0^{(2)}(\xi,\zeta,\tau) + \varepsilon u_1^{(2)}(\xi,\zeta,\tau) + \cdots\}.$$

From the continuity equation (2.19), we find appropriate expansion of w

$$w^{(2)}(\xi,\zeta,\tau) = w_0^{(2)}(\xi,\zeta,\tau) + \varepsilon w_1^{(2)}(\xi,\zeta,\tau) + \cdots.$$

In addition, we assume large surface tension (to be comparable with hydrostatic pressure and inertial effects) and define the unit-order parameter $S = \varepsilon^2\sigma$. We note that we have performed a similar expansion in Segin *et al.* (2004) without allowing for gas compressibility. In addition, a similar expansion was performed by Tilley *et al.* (1994a) without the assumption of a particular scaling of the viscosities and the densities.

From the equation of state, along with the z-component of the momentum equations, we can recover the incompressible limit if K is sufficiently large. We are interested in the case, however, when pressure gradients (equivalently density gradients) in the gas are comparable to those found in the liquid. Based on the analysis of the incompressible case (Segin *et al.*, 2004), we know that the liquid pressure must scale as $p^{(1)} = \mathrm{O}(1/\varepsilon)$ in order for pressure gradients to drive the x-component of the fluid velocity at leading order. From the ideal gas law, a gas pressure of $\mathrm{O}(1/\varepsilon)$ results in a scaling for $K = D/\varepsilon^3$, $D = \mathrm{O}(1)$ (see (2.10) and the text that follows for the definition of K). This choice of scaling results in the following asymptotic expansion for the pressure in each phase:

$$p^{(i)}(\xi,\zeta,\tau) = \frac{1}{\varepsilon}\{p_0^{(i)}(\xi,\zeta,\tau) + \varepsilon p_1^{(i)}(\xi,\zeta,\tau) + \cdots\}, \quad i = 1, 2.$$

From (2.6)–(2.15), we obtain the following sequence of linear problems:

$$\mathrm{O}(\varepsilon^{-1}): \quad p_{0\zeta}^{(i)} = 0, \tag{2.22}$$

$$\underline{\zeta = h(\xi,\tau)}: \quad p_0^{(1)} = p_0^{(2)}, \tag{2.23}$$

$$\mathrm{O}(1): \quad -p_{0\xi}^{(2)} + \mu u_{0\zeta\zeta}^{(2)} = 0, \tag{2.24}$$

$$-p_{0\xi}^{(1)} + \sin\beta + u_{0\zeta\zeta}^{(1)} = 0, \tag{2.25}$$

$$p_{1\zeta}^{(1)} + \cos\beta = 0, \tag{2.26}$$

$$p_{1\zeta}^{(2)} = 0, \tag{2.27}$$

$$u_{0\xi}^{(1)} + w_{0\zeta}^{(1)} = 0, \tag{2.28}$$

$$(\rho u_0^{(2)})_\xi + (\rho w_0^{(2)})_\zeta = 0, \tag{2.29}$$

$$\underline{\zeta = h(\xi,\tau)}: \quad u_0^{(2)} = 0, \tag{2.30}$$

$$\mu u_{0\zeta}^{(2)} - u_{0\zeta}^{(1)} = 0, \tag{2.31}$$

$$p_1^{(1)} - p_1^{(2)} = -Sh_{\xi\xi}, \tag{2.32}$$

$$w_0^{(2)} - h_\xi u_0^{(2)} = 0, \tag{2.33}$$

$$\underline{\zeta = 0}: \quad u_0^{(1)} = 0, \tag{2.34}$$

$$w_0^{(1)} = 0, \tag{2.35}$$

$$\underline{\zeta = 1}: \quad u_0^{(2)} = 0, \tag{2.36}$$

$$w_0^{(2)} = 0. \tag{2.37}$$

From equations $\mathrm{O}(\varepsilon^{-1})$, (2.22) and (2.23), we find that

$$p_0^{(1)}(\xi,\tau) = p_0^{(2)}(\xi,\tau) = p_0(\xi,\tau).$$

The O(1) $z(\zeta)$-momentum equations, (2.26) and (2.27), with Condition (2.32) on the interface yield

$$p_1^{(1)}(\xi,\zeta,\tau) = -(\cos\beta)\zeta + P_1(\xi,\tau)$$

and

$$p_1^{(2)}(\xi,\tau) = -h(\xi,\tau)\cos\beta + P_1(\xi,\tau) + Sh_{\xi\xi}.$$

In what follows, we refer to (as of now an unknown function) $P_1(\xi,\tau)$ as the pressure correction.

The O(1) $x(\xi)$-momentum equations, (2.24), (2.25), continuity equations (2.28), (2.29) with the boundary conditions (2.34)–(2.37) and continuity of the tangential component of the velocity and shear

stress at interface (2.30), (2.31) yield

$$u_0^{(1)} = \frac{p_{0\xi} - \sin\beta}{2}\zeta^2 + \frac{2h\sin\beta - (h+1)p_{0\xi}}{2}\zeta, \tag{2.38}$$

$$w_0^{(1)} = -\frac{p_{0\xi\xi}}{6}\zeta^3 + \left\{-h_\xi \sin\beta + \frac{p_{0\xi\xi}}{2}(h+1) + p_{0\xi}\frac{h_\xi}{2}\right\}\frac{\zeta^2}{2}, \tag{2.39}$$

$$u_0^{(2)} = \frac{p_{0\xi}}{2\mu}(\zeta-1)^2 + \frac{p_{0\xi}(1-h)}{2\mu}(\zeta-1), \tag{2.40}$$

$$w_0^{(2)} = -\frac{(\rho p_{0\xi})_\xi}{6\rho\mu}(\zeta-1)^3 + \frac{(\rho p_{0\xi}[h-1])_\xi}{4\rho\mu}(\zeta-1)^2. \tag{2.41}$$

The details of this procedure at $O(\varepsilon)$ are given in Appendices A and B. Based on this analysis, continuity of the normal velocity (2.13) gives the equation for the pressure gradient, while the interfacial shape is found using the kinematic boundary condition (2.15)

$$-\left[\frac{\rho p_\xi^{(2)}(1-h)^3}{12\mu}\right]_\xi + \varepsilon\left(\rho_\tau(1-h) + \frac{h(h+2)}{4}\rho h_\xi\sin\beta + \frac{h^2(1-h)}{4}\rho_\xi\sin\beta\right)$$
$$+\varepsilon\left\{\frac{h^2(h+3)}{12}\rho_\xi p_\xi - \frac{(1+h)^2}{4(1-h)}\rho h_\xi p_\xi + \mathrm{Re_l}T\right\} = 0, \tag{2.42}$$

$$h_\tau + A_{1\xi} + \varepsilon\left(S\frac{h^3}{3}h_{\xi\xi\xi} - \frac{h^3}{3}h_\xi\cos\beta + A_2 + \mathrm{Re_l}I\right)_\xi = 0, \tag{2.43}$$

$$p^{(2)} = D\rho, \tag{2.44}$$

where

$$A_1 = \frac{h^3}{3}\sin\beta - \frac{h^2(h+3)}{12}p_\xi^{(2)},$$

$$A_2 = \frac{\mu h^3 p_\xi}{4(1-h)} - \frac{\mu h^4}{4(1-h)}\sin\beta,$$

$$I = \frac{h^4(7h+25)}{240}p_{\xi\tau} + \frac{13}{480}h^2(1-h)^4\frac{\rho}{\mu^2}p_\xi\left\{-h_\xi p_\xi + \frac{\rho_\xi}{\rho}p_\xi(1-h)\right\}$$
$$-\frac{h^5(10h^2+7h+77)}{3360(1-h)}h_\xi p_\xi^2 + \frac{2}{15}h^6 h_\xi\sin^2\beta - \frac{h^5(29h^2+161h-378)}{20160}\frac{\rho_\xi}{\rho}p_\xi^2$$
$$+\sin\beta\left[\frac{h^6(109h+147)}{10080}\frac{\rho_\xi}{\rho}p_\xi + \frac{h^5(41h^2-49h-56)}{840(1-h)}p_\xi h_\xi\right],$$

$$T = -\frac{17}{3360\mu^3}[\rho^2 p_\xi^2(1-h)^6 h_\xi - \rho\rho_\xi p_\xi^2(1-h)^7]_\xi.$$

This system (2.42), (2.43) is closed using the appropriate boundary conditions. In the evolution equation (2.43), we require that the first and third derivatives vanish at both ends of the domain. This choice of

boundary conditions is motivated by its simplicity and by the fact that we consider only the flow far from the entrance and the exit. In the density equation (2.42), we prescribe $\rho(0,t)=\rho_{\text{in}}$ and $\rho(1,t)=\rho_{\text{out}}$, therefore also prescribing the pressure drop ($\Delta P = D[\rho_{\text{out}}-\rho_{\text{in}}]$).

We note that the asymptotic analysis ceases to be valid when (i) the leading-order term in the density equation (2.42) becomes comparable with the third term at order $\mathrm{O}(\varepsilon)$ and (ii) A_1 and εA_2 in the evolution equation (2.43) become comparable (since pressure gradient is proportional to $1/(1-h)^3$). This occurs when

$$\frac{1}{(1-h)^3} \sim \frac{\varepsilon}{(1-h)^6},$$

i.e. when $h \sim 1-\varepsilon^{1/3}$. Therefore, we consider only smaller values of h.

From the leading-order pressure gradient/density equation (2.42), we find that

$$(\rho_0^2)_\xi = \frac{2C(\tau)}{(1-h)^3}$$

for the density basic state, where $C(\tau)$ is a function of time resulting from integration. It is related to gas mass flow rate $q=\int_h^1 \rho u_0^{(2)}\,\mathrm{d}\zeta$ by $C(\tau)=-12\mu q$. Given the boundary conditions for ρ, we solve this equation explicitly to obtain

$$\rho_0^2(\xi) = \bar{Y}\rho_{\text{out}}^2 + (1-\bar{Y})\rho_{\text{in}}^2, \tag{2.45}$$

where

$$\bar{Y} = \frac{Y(\xi)}{Y(1)}, \quad Y(\xi) = \int_0^\xi \frac{1}{(h-1)^3}\,\mathrm{d}\xi'.$$

Note that this density base state is spatially dependent, even to the leading order. We later discuss the consequences of this spatial dependence on the methods that we use to approach the linear stability analysis.

At $\mathrm{O}(\varepsilon)$ from the pressure gradient/density equation (2.42) we find that the correction to density is given by

$$\begin{aligned}\rho_1(\xi) = &-\frac{1}{\rho_0(\xi)}\int_0^\xi \left[\frac{h_0^2\rho_0(\xi')\sin\beta}{4D(1-h_0)} + \frac{17}{3360}\frac{D}{\mu^3}(1-h_0)^4\rho_0\rho_{0_{\xi'}}^3\right]\mathrm{d}\xi' \\ &-\frac{1}{\rho_0(\xi)}\int_0^\xi \frac{h_0^2(h_0+3)}{12(1-h_0)^3}\int_0^{\xi'}\rho_{0_{\hat{\xi}}}\,\mathrm{d}\hat{\xi}\,\mathrm{d}\xi'.\end{aligned} \tag{2.46}$$

Before proceeding with the linear stability analysis of the system (2.42),(2.43), we consider the limit $\rho_\xi \to 0$ and $\rho_\tau \to 0$ and pressure being a function of spatial coordinates only (independent of density). This system of equations then models the incompressible flow and simplifies to the following form:

$$\begin{aligned}&-\left[\frac{\rho p_{0_\xi}(1-h)^3}{12\mu}\right]_\xi + \varepsilon\left(\frac{h(h+2)}{4}\rho h_\xi\sin\beta - \left[\frac{\rho p_{1_\xi}^{(2)}(1-h)^3}{12\mu}\right]_\xi\right) \\ &+\varepsilon\left\{-\frac{(1+h)^2}{4(1-h)}\rho h_\xi p_\xi - \mathrm{Re_l}\frac{17}{3360\mu^3}\left[\rho^2 p_\xi^2(1-h)^6 h_\xi\right]_\xi\right\} = 0,\end{aligned} \tag{2.47}$$

$$h_\tau + \hat{A_1}_\xi + \varepsilon\left(S\frac{h^3}{3}h_{\xi\xi\xi} - \frac{h^3}{3}h_\xi\cos\beta + A_2 + \mathrm{Re_l}\hat{I}\right)_\xi = 0, \tag{2.48}$$

where

$$\hat{A}_1 = \frac{h^3}{3}\sin\beta - \frac{h^2(h+3)}{12}p_{0\xi},$$

$$A_2 = \frac{\mu h^3 p_\xi}{4(1-h)} - \frac{\mu h^4}{4(1-h)}\sin\beta,$$

$$\hat{I} = \frac{h^4(7h+25)}{240}p_{\xi\tau} - \frac{13}{480}h^2(1-h)^4\frac{\rho}{\mu^2}p_\xi^2 h_\xi - \frac{h^5(10h^2+7h+77)}{3360(1-h)}h_\xi p_\xi^2$$

$$+\frac{2}{15}h^6 h_\xi \sin^2\beta + \sin\beta\frac{h^5(41h^2-49h-56)}{840(1-h)}p_\xi h_\xi - \left[\frac{h^2(h+3)}{12}p_{1\xi}^{(2)}\right].$$

This formulation reduces to simpler cases that do not include the effects of liquid inertia and/or pressure gradient (see Benjamin, 1957; Benney, 1966; Yih, 1967; Chang, 1986; Oron *et al.*, 1997; Segin *et al.*, 2004; Tilley *et al.*, 1994a,b). We will discuss further the connection of the linear stability analysis of the obtained presentation to the existing results in Section 3.

3. Linear stability theory for compressible two-phase flow

In Part 3.1 of this section, we outline the incompressible case. Then, in Part 3.2, we consider the compressible case $\rho_{\text{in}} = \rho_{\text{out}}$ with no applied pressure drop ($\Delta P = 0$), which is amenable to a normal-mode analysis. Section 3.3 considers the general case that includes the density difference/pressure jump along the channel. Here, we consider a vertical channel and use $\mu = 1$, $\rho_1 = 1$, $S = 3$ and $\varepsilon = 0.01$.

3.1 *Linear stability analysis for incompressible flow*

The comparison of the incompressible flow problem to the general case provides an insight into the influence of compressibility on the interfacial dynamics. Linear stability analysis of a two-layer incompressible system was considered by Charru & Fabre (1994) and Tilley *et al.* (1994a). We note that Tilley *et al.* (1994a) consider the flow with the constraint of constant flow rate, while here we concentrate on flow driven by a prescribed pressure drop ΔP, which is an experimentally realizable configuration. Despite this difference, the linear stability is similar in both cases and based on normal-mode expansion, as outlined below. Furthermore, one can easily transform from one configuration to the other by using the relation

$$\Delta P = \frac{12\mu q}{(1-h_0)^3},$$

where h_0 is the fixed basic interfacial height (the same for constant ΔP and constant q).

The linear stability analysis is performed by applying the expansion

$$h(\xi,\tau) = h_0 + \delta_0\, \mathrm{e}^{\mathrm{i}k(\xi - c\tau)} \tag{3.1}$$

in (2.47)–(2.48) and assuming that the perturbation δ_0 is small. We obtain

$$kc_{\mathrm{r}} = k\left[h_0^2 \sin\beta + \frac{h_0(1+h_0)}{2(1-h_0)}\Delta P + \varepsilon\frac{\mu}{4}\left(\frac{h_0^3(4-3h_0)}{(1-h_0)^2}\sin\beta - \frac{h_0^2(3+h_0)}{(1-h_0)^2}\Delta P\right)\right],$$

$$kc_{\mathrm{i}} = \varepsilon k^2\left[\mathrm{Re_l} I(\Delta P) - \frac{h_0^3}{3}\cos\beta - \frac{S}{3}h_0^3 k^2\right],$$

$$I(\Delta P) = D_1(\Delta P)^2 + D_2\Delta P + D_3,$$

$$\begin{aligned} D_1 &= \frac{h_0^5(5h_0^3 + 72h_0^2 + 371h_0 + 224)}{1680(1-h_0)^2} \\ &\quad + \frac{\rho}{\mu^2}\frac{h_0^2(1 - 15h_0^2 + 40h_0^3 - 35h_0^4 + 24h_0^5 + 5h_0^6)}{1680(1-h_0)^2}, \\ D_2 &= \frac{h_0^5(65h_0^2 + 623h_0 + 112)}{1680(1-h_0)}\sin\beta, \\ D_3 &= \frac{2}{15}h_0^6\sin^2\beta, \end{aligned} \tag{3.2}$$

where periodic boundary conditions are assumed. The same expression follows from Tilley *et al.* (1994a), if one assumes the particular scaling of densities and viscosities that is employed in this work.

If inertial effects are ignored ($\mathrm{Re_l} = 0$), and hydrostatic effects are not destabilizing ($\cos\beta \geqslant 0$) the flow is always stable. Figure 2 shows the stability diagram resulting from (3.2) in the more interesting case, where inertial effects are present ($\mathrm{Re_l} > 0$). Here, we observe that the flow is destabilized under sufficient shear, with the stability boundaries nearly symmetric under $\Delta P \leftrightarrow -\Delta P$. This approximate symmetry is due to the fact that the dominant term in the definition of $I(\Delta P)$ (see (3.2)) is D_1, which is $\mathrm{O}(h_0^2)$, while the rest of the terms are of $\mathrm{O}(h_0^5)$, or higher. However, the slight asymmetry leads to instabilities in the limit of vanishing k and ΔP, viz. Fig. 2. Therefore, an incompressible flow without applied pressure drop is 'unstable' for small wave numbers. We discuss whether this result extends to the compressible case in Section 3.2.

3.2 *Normal-mode analysis for compressible case ($\rho_{\mathrm{in}} = \rho_{\mathrm{out}}$)*

The special case $\rho_{\mathrm{in}} = \rho_{\mathrm{out}}$ (corresponding to $\Delta P = 0$) allows for normal-mode analysis. Here, we also apply periodic boundary conditions and expand

$$h(\xi,\tau) = h_0 + \delta_0\,\mathrm{e}^{\mathrm{i}k(\xi - c\tau)},$$

$$\rho_0(\xi,\tau) = \bar{\rho}_0(\xi) + \Delta_0\,\mathrm{e}^{\mathrm{i}k(\xi - c\tau)},$$

where $\bar{\rho}_0(\xi) = \rho_0(\xi) + \varepsilon\rho_1(\xi)$. When $\rho_{\mathrm{in}} = \rho_{\mathrm{out}}$, the correction to base density state vanishes and we obtain $\rho_0(\xi) = \bar{\rho}_0(\xi) = \rho_{\mathrm{in}}$ (note that the base state gas flow has constant density, but compressible

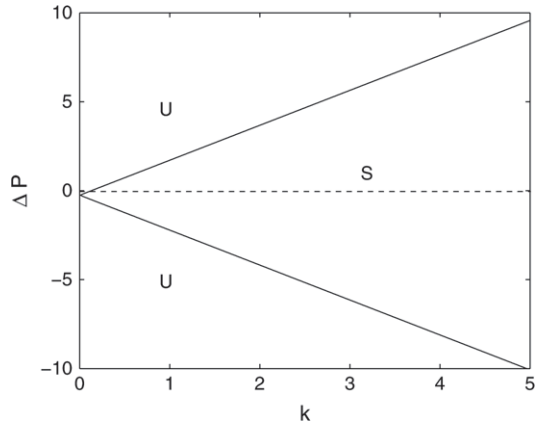

FIG. 2. Neutral stability curves for incompressible two-layer flow for $h_0 = 0.5$, $\mu = 1$, $\rho_1 = 1$, $\beta = \pi/2$, $S = 3$, $\varepsilon = 0.01$ and $\mathrm{Re}_\mathrm{l} = 1$. Unstable regions are denoted by 'U' and stable regions by 'S'.

effects are present in the disturbance). After substituting these expansions into (2.42), (2.43), we arrive at the following system of characteristic equations:

$$-\mathrm{i}kc\varepsilon\,\Delta_0 + \mathrm{i}ka_2\delta_0 + \mathrm{i}ka_4\Delta_0 + (\mathrm{i}k)^2 a_5\Delta_0 = 0, \tag{3.3}$$

$$-\mathrm{i}kc\delta_0 - (\mathrm{i}k)^3 c\alpha\,\Delta_0 + b_1(\mathrm{i}k)^2\Delta_0 + \mathrm{i}kb_3\delta_0 + (\mathrm{i}k)^2 b_4\delta_0 + b_5(\mathrm{i}k)^4\delta_0 = 0, \tag{3.4}$$

where k is the wave number, and

$$a_2 = \varepsilon\frac{h_0(h_0+2)}{4(1-h_0)}\rho_0\sin\beta, \quad a_4 = \varepsilon\frac{h_0^2}{4}\sin\beta, \quad a_5 = -\frac{D(1-h_0)^2}{12\mu}\rho_0,$$

$$b_1 = -\frac{D}{12}h_0^2(h_0+3) + \varepsilon\frac{\mu D h_0^3}{4(1-h_0)}, \quad b_3 = h_0^2\sin\beta - \frac{\varepsilon\mu}{4}\sin\beta\frac{h_0^3(4-3h_0)}{(1-h_0)^2},$$

$$b_4 = -\varepsilon\frac{h_0^3}{3}\cos\beta + \frac{2\varepsilon\mathrm{Re}_\mathrm{l}}{15}h_0^6\sin^2\beta, \quad b_5 = \varepsilon\frac{S}{3}h_0^3,$$

$$\alpha = \frac{D}{240}h_0^4(7h_0+25).$$

Thus, we obtain a system of two coupled equations (3.3), (3.4), which we solve to find kc; the growth rate is given by the imaginary part of this quantity.

For $D = 0$, the interfacial perturbation δ_0 in system (3.3), (3.4) does not depend on the density perturbation Δ_0, but Δ_0 depends on δ_0. In this limit, the gas dynamics are slaved to the interfacial dynamics, and hence the stability of the system is governed by the stability of the interfacial dynamics. In this case, the system of equations (3.3) and (3.4) simplifies to

$$-\mathrm{i}kc\delta_0 + \mathrm{i}kb_3\delta_0 + (\mathrm{i}k)^2 b_4\delta_0 + b_5(\mathrm{i}k)^4\delta_0 = 0, \tag{3.5}$$

$$-\mathrm{i}kc\,\Delta_0 + \mathrm{i}ka_2\delta_0 + \mathrm{i}ka_4\Delta_0 = 0. \tag{3.6}$$

From (3.5), we obtain the same growth rate for the interfacial height as in the incompressible case (viz. (3.2) for $\Delta P = 0$; see also Segin, 2004)

$$kc_{\mathrm{i}} = \varepsilon k^2 \left[-\tfrac{S}{3} h_0^3 k^2 - \tfrac{h_0^3}{3} \cos\beta + \tfrac{2}{15} \mathrm{Re}_{\mathrm{l}} h_0^6 \sin^2\beta \right], \tag{3.7}$$

$$kc_{\mathrm{r}} = k \left[h_0^2 \sin\beta + \varepsilon \tfrac{\mu}{4} \tfrac{h_0^3(4-3h_0)}{(1-h_0)^2} \sin\beta \right]. \tag{3.8}$$

Here, from (3.7) we obtain that short wavelengths are stabilized by capillarity, hydrostatic effects are stabilizing for $\beta < \pi/2$ and the flow is destabilized by inertial effects. Therefore, although not physical, we find that when $\Delta P = 0$ the limit $D = 0$ corresponds to the incompressible case characterized by passive gas response. The phase speed (3.8) is determined primarily by advection and instabilities propagate with a speed proportional to h_0^2.

From (3.6), after division by ik, we obtain the characteristic equation for the density mode. Since a_2 and a_4 in this characteristic equation are real coefficients, we note that the growth rate for the density mode (defined by the imaginary part of c) is not affected by its deviation from the interfacial profile. However, the density phase speed does depend on the basic interfacial height h_0 and the deviation from it, δ_0.

When $D \neq 0$, the density and interfacial modes are coupled. If we assume that the interface is flat ($\delta_0 = 0$), then the density mode is stable, as can be verified from (3.3). Indeed, the density growth rate is given by

$$kc_{\mathrm{i}} = -\frac{D(1-h_0)^2}{12\varepsilon\mu} \rho_0 k^2, \tag{3.9}$$

showing stability.

When the interfacial deviations are non-zero ($\delta_0 \neq 0$), we proceed with the general case defined by (3.3) and (3.4). First we note that, similar to the incompressible case, the flow characterized by $\mathrm{Re}_{\mathrm{l}} = 0$ is always stable. Therefore, we concentrate on the $\mathrm{Re}_{\mathrm{l}} > 0$ case, and solve (3.3) and (3.4) numerically.

Figure 3 presents the resulting growth rates for the interfacial and density modes. In Fig. 3(a), which shows interfacial growth rate (the incompressible case is calculated using (3.7)), we see that compressibility effects 'stabilize' the flow. In particular, for small k's shown in Fig. 3, the stability changes from unstable for $D = 0$ (see Fig. 2) to stable for $D > 0$. Furthermore, this stabilizing effect is stronger for larger D's. Figure 3(b) shows the density mode, which is stable for all D's. Figure 4 presents the phase speeds. Here, we observe a relatively weak, but a noticeable effect of compressibility. An increase of D leads to a decrease of the interfacial phase speed (part a), but also to an increase of the phase speed of the density mode (part b).

To conclude, if $\rho_{\mathrm{in}} = \rho_{\mathrm{out}}$, corresponding to $\Delta P = 0$, we see a 'stabilizing' effect of compressibility. Next, we proceed with examining the influence of compressibility on a two-fluid flow in the general case where $\rho_{\mathrm{out}} \neq \rho_{\mathrm{in}}$.

3.3 *Linear stability for a general case ($\rho_{\mathrm{out}} > \rho_{\mathrm{in}}$)*

If we relax the assumption of equal values of densities at the ends of the domain, we need to approach the stability problem more generally. In particular, periodic boundary conditions used in normal-mode analysis are not appropriate, so we concentrate on the channel of fixed length. In order to test our

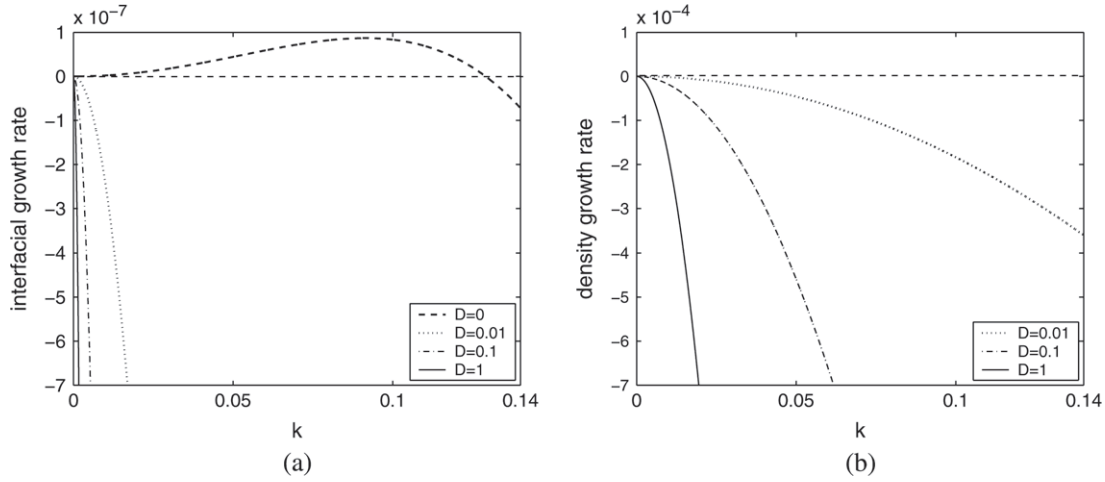

FIG. 3. Growth rate curves for (a) interfacial mode and (b) density mode versus wave number for $\rho_{\text{out}} = 1$, $h_0 = 0.5$, $\text{Re}_{\text{l}} = 1$ and for different values of D.

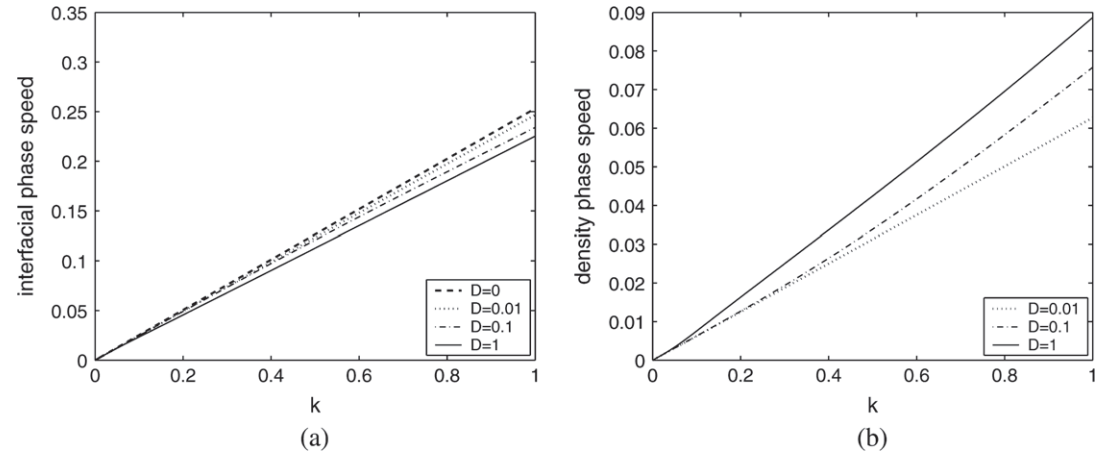

FIG. 4. Phase speed for (a) interfacial mode and (b) density mode versus wave number for $\rho_{\text{out}} = 1$, $h_0 = 0.5$, $\text{Re}_{\text{l}} = 1$ and for different values of D (note different range of k compared to the preceding figure).

approach to this problem, we consider the $\rho_{\text{in}} = \rho_{\text{out}}$ case with an interval of length 2π and perturb the interfacial height and density

$$h(\xi, \tau) = h_0 + \delta(\xi)\mathrm{e}^{\sigma\tau}, \tag{3.10}$$

$$\rho_0(\xi, \tau) = \bar{\rho}_0(\xi) + \Delta(\xi)\mathrm{e}^{\sigma\tau}, \tag{3.11}$$

where $\delta(\xi)$, $\Delta(\xi) \ll \varepsilon$, $\bar{\rho}_0(\xi) = \rho_0(\xi) + \varepsilon\rho_1(\xi)$. The base density state can be found from (2.45) and the correction to it from (2.46) using $h(\xi, \tau) = h_0$

$$\rho_0^2(\xi) = \xi\rho_{\text{out}}^2 + (1 - \xi)\rho_{\text{in}}^2, \tag{3.12}$$

$$\rho_1(\xi) = -\frac{h_0^2 \sin\beta}{6D\rho_0(\xi)(1-h_0)} \frac{[\{(\rho_{\text{out}}^2 - \rho_{\text{in}}^2)\xi + \rho_{\text{in}}^2\}^{\frac{3}{2}} - \rho_{\text{in}}^3]}{\rho_{\text{out}}^2 - \rho_{\text{in}}^2}$$
$$- \frac{17}{26880} \frac{D(1-h_0)^4}{\mu^3 \rho_0(\xi)} (\rho_{\text{out}}^2 - \rho_{\text{in}}^2)^2 \ln\left(1 + \left\{\frac{\rho_{\text{out}}^2}{\rho_{\text{in}}^2} - 1\right\}\xi\right)$$
$$- \frac{h_0^2(h_0+3)(\rho_{\text{out}}^2 - \rho_{\text{in}}^2)}{48\rho_0(\xi)(1-h_0)^3} \left[\left(\xi + \frac{\rho_{\text{out}}^2}{\rho_{\text{in}}^2} - 1\right) \ln\left\{1 + \left(\frac{\rho_{\text{out}}^2}{\rho_{\text{in}}^2} - 1\right)\xi\right\} - \xi\right]. \quad (3.13)$$

Figure 5 shows the basic density state ($\rho_0(\xi)$) and the correction to it ($\rho_1(\xi)$). We immediately observe that $|\rho_1(\xi)| \ll \rho_0(\xi)$; however, for completeness we include it in the analysis below.

After substituting the expansion (3.10), (3.11) into the linearized system of equations (2.42), (2.43) and using (3.12) and (3.13) we arrive at the system of characteristic equations

$$\sigma\delta + \sigma\alpha\Delta_{\xi\xi} + \bar{b}_6\Delta + \bar{b}_7\Delta_\xi + \bar{b}_1\Delta_{\xi\xi} + \bar{b}_2\delta + \bar{b}_3\delta_\xi + \bar{b}_4\delta_{\xi\xi} + b_5\delta_{\xi\xi\xi\xi} = 0, \quad (3.14)$$

$$\sigma\Delta + \bar{a}_1\delta + \bar{a}_2\delta_\xi + \bar{a}_6\delta_{\xi\xi} + \bar{a}_3\Delta + \bar{a}_4\Delta_\xi + \bar{a}_5\Delta_{\xi\xi} = 0. \quad (3.15)$$

Appendix C gives the definitions of the coefficients. We resolve (3.14), (3.15) numerically using a second-order accurate finite-difference method in space (central differencing). This procedure leads to the following generalized eigenvalue problem:

$$\mathbf{A}\mathbf{x} + \sigma\mathbf{B}\mathbf{x} = 0,$$

where $\mathbf{A}$ is a matrix of coefficients resulting from the spatial discretization, $\mathbf{B}$ is the matrix formed by the coefficients multiplying σ and vector $\mathbf{x}$ is a column of unknowns $(\delta_1, \ldots, \delta_N, \Delta_1, \ldots, \Delta_N)$.

We perform the power method (Strang, 1988) on the matrix $\mathbf{B}^{-1}\mathbf{A}$ to find the growth rate for a given wavenumber. Table 1 shows the results of this procedure compared with the results of the normal-mode analysis. For small wavenumbers, we find good agreement, therefore justifying the use of the power method. We note in passing that such a good agreement is not as easily obtained for higher

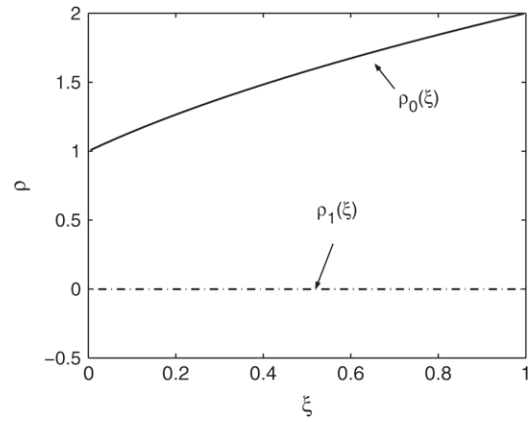

FIG. 5. Density profiles: basic state ($\rho_0(\xi)$) and the correction $\rho_1(\xi)$, for $h_0 = 0.1$, $\rho_{\text{out}} = 2$, $D = 1$ and $\text{Re}_{\text{l}} = 0$.

TABLE 1 *Growth-rate comparison between the power method and normal-mode analysis for* $\rho_{\text{out}} = 1$, $h_0 = 0.5$, $\text{Re}_\text{l} = 1$ *and* $D = 1$. *We use a grid with* $N = 64$ *points to approximate growth rate for the wave number* $k = 1$ *and* $N = 128$ *for* $k = 2$

Wave number	Power method	Normal modes
1	−2.081660	−2.081644
2	−8.3266	−8.3316

wavenumbers since the method is more prone to numerical instabilities, due to a large condition number of the matrix **A**.

As an additional test, the computations have been also carried out using the iterative shifted inverse power method (Strang, 1988). The inverse power method is performed on the matrix $\mathbf{A^{-1}B}$; an advantage of this method is that one does not need to find the inverse of the sparse matrix **B**. In order to increase the rate of convergence, we implemented the iterative scheme with the matrix $\mathbf{A^{-1}B} - \mu I$, where μ is the shifted value for all eigenvalues, obtained by solving $\mathbf{Ax} = -\mu\mathbf{Bx}$. For all considered cases, the agreement between the two methods is excellent.

We next apply the power method to the general case, where $\rho_{\text{in}} \neq \rho_{\text{out}}$. In order to better understand the influence of the compressibility of the gas we first consider in Section 3.3.1 the system where inertial effects are ignored, and then include these effects in Section 3.3.2.

3.3.1 *Linear stability analysis without inertial effects.* For $\text{Re}_\text{l} = 0$, the system of characteristic equations (3.14) and (3.15) reduces to

$$\sigma\delta + b_1\Delta_{\xi\xi} + b_2\delta + b_3\delta_\xi + b_4\delta_{\xi\xi} + b_5\delta_{\xi\xi\xi\xi} = 0, \tag{3.16}$$

$$\sigma\Delta + a_1\delta + a_2\delta_\xi + a_3\Delta + a_4\Delta_\xi + a_5\Delta_{\xi\xi} = 0, \tag{3.17}$$

where the definitions of the a_i's and b_i's are given in Appendix C.

Figure 6 presents the dependence of the maximum growth rate on the parameter D for a few different cases. We note that $D = 0$ corresponds to the incompressible limit, which is always stable for $\text{Re}_\text{l} = 0$. Non-zero D's may, however, lead to instability. Therefore, these results imply that compressibility may 'destabilize' the flow.

Figure 6 shows that instability develops as either ρ_{out} or h_0 are increased. For example, if we fix $\rho_{\text{out}} = 2$, we see that an increase of h_0 modifies drastically the dynamics of the flow as D is increased: from stable flow ($h_0 = 0.1$) to unstable ($h_0 = 0.5$). Here, we expect that the observed behaviour of the maximum growth rate results from the competition between advection (due to the significant value of the induced driving force) and capillarity. At the cutoff value of D ($\approx$3.7 for $\rho_{\text{out}} = 2$ and $h_0 = 0.5$), these two mechanisms balance each other. When we fix $h_0 = 0.5$, and change ρ_{out} from 2 (solid line) to 5 (dashed line), we observe that instabilities develop at smaller values of D for larger ρ_{out}. We note in passing that the growth rates shown in Fig. 6 are much larger in their absolute value compared to the growth rates in the case $\rho_{\text{in}} = \rho_{\text{out}}$ shown in Fig. 3; this illustrates the fact that for our choice of parameters, the stability of the interface is predominantly determined by the imposed gas flow.

3.3.2 *Linear stability analysis including inertial effects.* We proceed with the inclusion of inertial effects. Note that in single-phase liquid films, the liquid inertia is the source of linear instability in the long-wave regime (Benjamin, 1957; Yih, 1967).

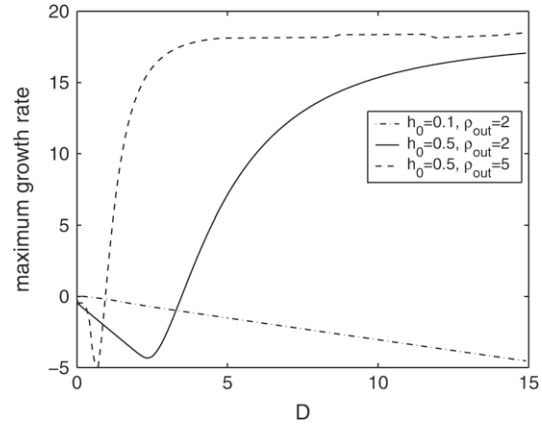

FIG. 6. Dependence of the maximum growth rate on D for $\mathrm{Re}_l = 0$.

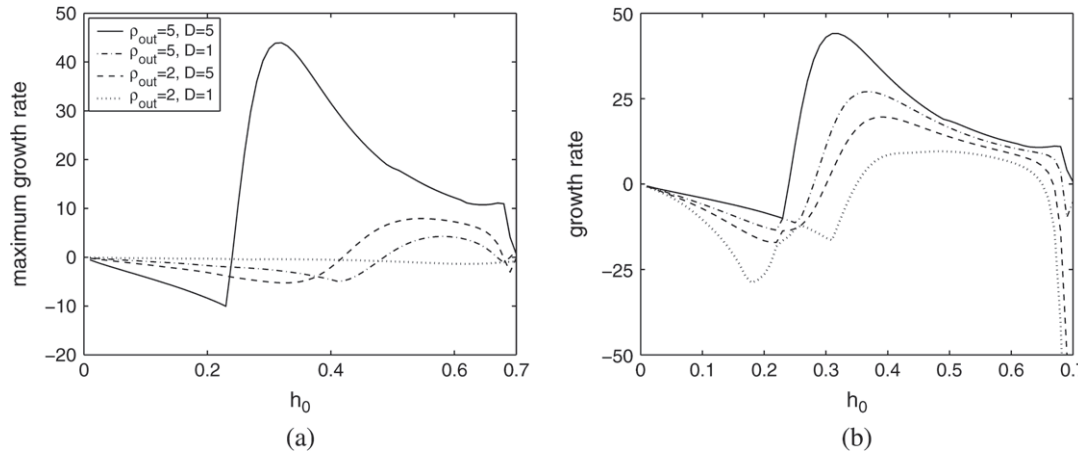

FIG. 7. (a) The growth rate of the most unstable mode versus interfacial height for $\mathrm{Re}_l = 1$. Sharp corner in the growth rate for $\rho_{\mathrm{out}} = 5$, $D = 5$ correspond to the crossing eigenvalues. (b) The growth rates of unstable modes for $\rho_{\mathrm{out}} = 5$, $D = 5$. The solid curve outlines the most unstable mode for a given h_0.

Figure 7(a) shows the maximum growth rates versus h_0 for four different combinations of ρ_{out} and D. The main features of the results are as follows: (i) for sufficiently small h_0, the flow is stable; (ii) this region of h_0 that corresponds to stability is decreased as ρ_{out} and/or D are increased.

Although these results are consistent with those presented in the previous sections, some features require more careful explanation. In particular, the presence of sharp 'corners' for $\rho_{\mathrm{out}} = 5$, $D = 5$, close to $h_0 = 0.23$ may appear surprising. More details of this particular case are presented in Fig. 7(b). We see that multiple unstable modes are present. Therefore, one 'jumps' from one unstable mode to another as one follows the most unstable mode through $h_0 = 0.23$. Figure 8, which shows the normalized spatial eigenfunction profiles that correspond to the maximum growth rate/eigenvalue in the vicinity of $h_0 = 0.23$, confirms this observation. The change of the eigenfunctions as h_0 is increased shows that we switch to a different eigenvalue close to $h_0 = 0.23$ as h_0 increases.

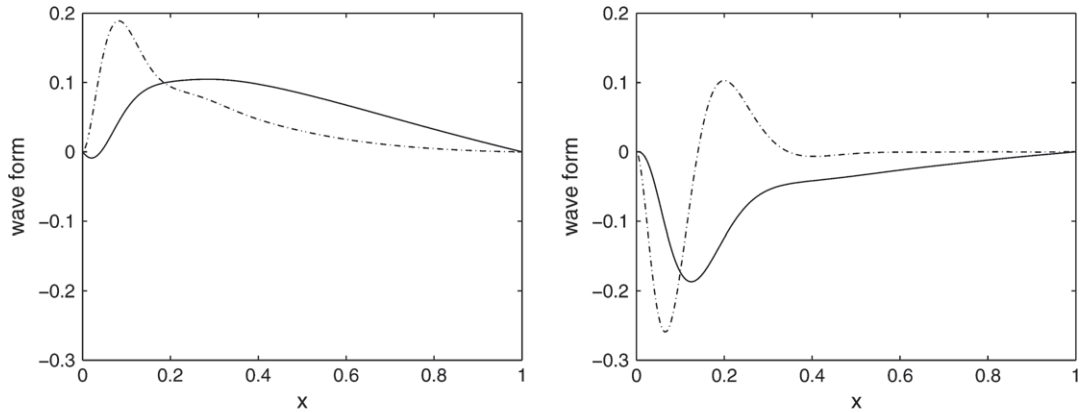

FIG. 8. Dependence of the form of the eigenfunction on the basic interfacial height for $\mathrm{Re_l} = 1$, $D = 5$, $\rho_{\mathrm{out}} = 5$. The interfacial mode is plotted as a dash-dotted line and density mode as a solid line; the eigenfunctions are normalized (L_2 norm $= 1$). The change in the shape of the eigenfunction corresponds to crossing eigenvalues and explains the sharp corner in the maximum growth rate plot shown in Fig. 7.

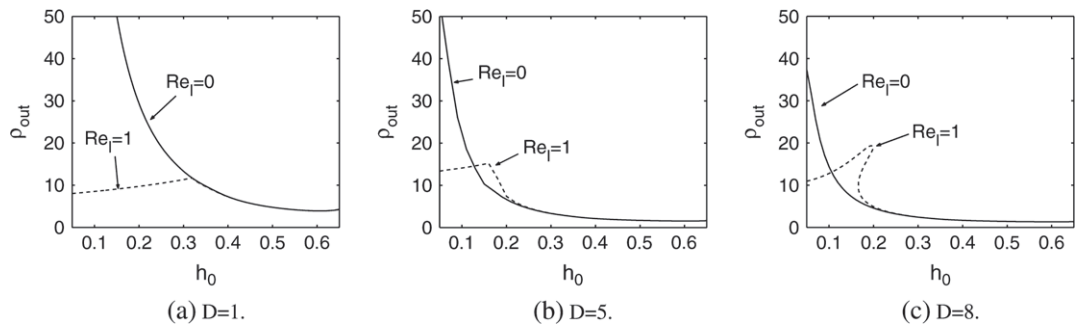

FIG. 9. Graphs of neutral stability curves for $\mathrm{Re_l} = 0$ and $\mathrm{Re_l} = 1$ for different values of D. The flow is stable below the neutral stability curves and unstable above them.

Next, we consider parametric plots obtained using a fixed parameter D, with the goal of understanding the influence of liquid inertia on the stability in more detail. Figure 9 shows neutral stability curves that separate the parameter space in stable (below the curves) and unstable (above the curves) regions. The main features of the results shown in this figure are as follows:

- Compressibility may lead to instability in the flow characterized by $\mathrm{Re_l} = 0$, which is always stable in the incompressible limit. Larger D's lead to a wider range of the parameter space $[h_0, \rho_{\mathrm{out}}]$ where the flow is unstable. However, rather strong driving $\rho_{\mathrm{out}} \gg \rho_{\mathrm{in}}$ is needed for this instability to occur.
- Similar to the incompressible limit, inertial effects destabilize the flow. Figure 9 shows that this effect is particularly relevant for small h_0's.

We compare the stability properties between the incompressible and the compressible case for $\mathrm{Re_l} > 0$. Since physical experiments typically control the pressure drop, and not the density, we replot

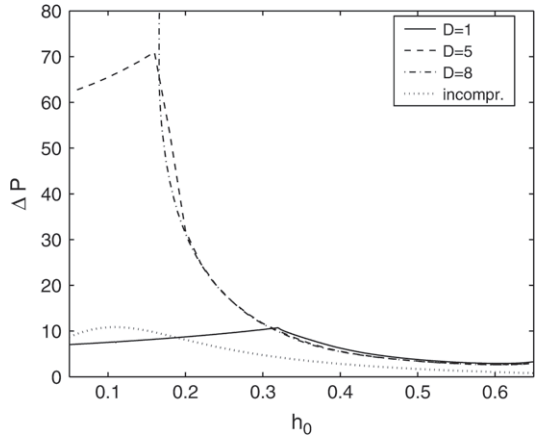

FIG. 10. Neutral stability curves in $\Delta P - h_0$ plane for $\mathrm{Re_l} = 1$. The flow is stable below the neutral stability curves and unstable above them.

the results from Fig. 9 for $\mathrm{Re_l} = 1$ in the $[h_0, \Delta P]$ space. This plot will additionally allow us to directly discuss the effect of compressibility on the stability of the flow, since ΔP is a well-defined quantity in the incompressible limit as well.

Figure 10 shows the neutral stability curves in $[h_0, \Delta P]$ space, including the incompressible limit. Similar to the results obtained for $\Delta P = 0$ (i.e. $\rho_{\mathrm{in}} = \rho_{\mathrm{out}}$, see Fig. 3) we find a stabilizing effect of compressibility, in particular for small values of h_0. This stabilizing effect of gas was also reported in Demekhin *et al.* (1989) who coupled an Orr-Sommerfeld problem in the semi-infinite gas to the linear stability analysis of the gas–liquid interface.

One may wonder why the influence of compressibility is different in the flows with and without inertial effects. One interpretation is that, under the assumptions of this work, in the incompressible limit the effect of gas flow is tied to the inertial response, see (3.2). Therefore, there is no influence of an imposed pressure drop and resulting shear stresses if $\mathrm{Re_l} = 0$. The compressible treatment relaxes this link between inertial effects and imposed shear, leading to potential instability. However, if the inertial effects are included, the interface typically becomes more stable under full compressible treatment, since the effect of imposed shear may be absorbed by the density modes, which is not the case under the incompressible limit.

4. Conclusions

We have investigated the non-linear evolution of the interface between two immiscible fluids in an inclined channel. Motivated by air–water systems, we employed a particular scaling of the gas/liquid viscosities and densities. This scaling allowed us to formulate a tractable problem, in which various effects, such as liquid inertia or gas compressibility, can be clearly understood.

Following this scaling, through a lubrication approximation we derive a system of non-linear evolution equations that governs the motion of the interface between the two fluids and the gas pressure. The lubrication approach includes the inertial effects of the liquid layer and the Reynolds stress terms in the gas. Although performing linear stability analysis for the compressible case is complicated by the fact that the base density state is spatially dependent, we are able to solve the resulting problem numerically and extract the influence of compressibility on the stability properties of the flow.

In the case of vanishing imposed pressure drop ($\Delta P = 0$), we find that compressibility removes long wavelength instability that is present in the incompressible flow for $\mathrm{Re_l} > 0$. Still for $\Delta P = 0$, and for $\mathrm{Re_l} = 0$, the flow is stable both with and without compressibility. For the flows where $\Delta P > 0$, we find that compressibility has more involved effects. Here, the flows characterized by $\mathrm{Re_l} = 0$ may be destabilized by compressibility effects, in particular for a strong driving force (i.e. large $\rho_{\mathrm{out}} - \rho_{\mathrm{in}}$ or large ΔP). This is due to the fact that in the incompressible case, the effect of ΔP on stability is present only for non-zero $\mathrm{Re_l}$, while this is not the case if compressibility effects are included. However, if $\mathrm{Re_l} > 0$, compressibility typically stabilizes the interface, i.e. it increases the region of the parameter space $[h_0, \rho_{\mathrm{out}} - \rho_{\mathrm{in}}]$ in which the flow is stable.

An interesting artifact of the presented results corresponds to the spatial behaviour of the density and interfacial disturbances (see Fig. 8). Interfacial deflections are localized near the inlet. One argument for the onset of flooding is the presence of a localized disturbance near the inlet prior to the event. These results suggest that a linear theory with the appropriate boundary conditions on the density and interfacial height at the liquid inlet and outlet may provide the criteria for the flooding event. This work focuses on one possible set of boundary conditions, but a matched asymptotic expansion local to the channel ends is needed to see if this approach can describe the flooding event. Future work will concentrate on this and other issues relevant to numerous applications of two-fluid flows.

REFERENCES

ALEXAKIS, A., YOUNG, Y. & ROSNER, R. (2002) Shear stability of fluid interfaces: stability analysis. *Phys. Rev. Lett. E*, **65**, 1–17.

BANKOFF, S. G. & LEE, S. C. (1986) *Multiphase Science and Technology. A Critical Review of the Flooding Literature.* Washington DC: Hemisphere.

BATCHELOR, G. K. (1967) *An Introduction to Fluid Dynamics*. New York: Cambridge University Press.

BENJAMIN, T. B. (1957) Wave formation in laminar flow down an inclined plane. *J. Fluid Mech.*, **2**, 554–574.

BENNEY, D. J. (1966) Long waves on liquid films. *J. Math. Phys. (N. Y.)*, **45**, 150–155.

BOUSMAN, W. S., MCQUILLEN, J. B. & WITTE, L. C. (1996) Gas-liquid flow patterns in microgravity: effects of tube diameter, liquid viscosity and surface tension. *Int. J. Multiphase Flow*, **22**, 1035–1053.

CHANG, H.-C. (1986) Nonlinear waves on liquid film surfaces. Part I: flooding in a vertical tube. *Chem. Eng. Sci.*, **41**, 2463–2476.

CHARRU, F. & FABRE, J. (1994) Long waves at the interface between two viscous fluids. *Phys. Fluids*, **6**, 1223–1235.

DEMEKHIN, E. A., TOKAREV, G. YU. & SHKADOV, V. YA. (1989) Instability and nonlinear waves on a vertical liquid film flowing counter to a turbulent gas flow. *Teor. Osn. Khim. Tekhnol.*, **23**, 64–70.

DUKLER, A. E., FABRE, J. A., MCQUILLEN, J. B. & VERNON, R. (1988) Gas liquid flow at microgravity conditions: flow patterns and their transitions. *Int. J. Multiphase Flow*, **14**, 389–400.

FABER, T. E. (2001) *Fluid Dynamics for Physicists*. New York: Cambridge University Press.

FOWLER, A. C. & LISSETER, P. E. (1992) Flooding and flow reversal in annular two-phase flows. *SIAM J. Appl. Math.*, **52**, 15–33.

HAGSTROM, T. & LORENZ, J. (1998) All-time existence of classical solutions for slightly compressible flows. *SIAM J. Math. Anal.*, **29**, 652–672.

KIRSHBERG, J., YERKES, K. & LIEPMANN, D. (2000) Demonstration of a micro-CPL based on MEMS fabrication technologies. *AIAA, Proceedings from the 35th Intersociety Energy Conversion Engineering Conference*, Vol. 2, pp. 1198–1204.

LIVESCU, D. (2003) Compressibility effects on the Rayleigh-Taylor instability growth between immiscible fluids. *Phys. Fluids*, **16**, 118–127.

MOUZA, A. A., PARAS, S. V. & KARABELAS, A. J. (2003) Incipient flooding in inclined tubes of small diameter. *Int. J. Multiphase Flow*, **29**, 1395–1412.

MUDAWAR, I. (2001) Assessment of high-heat thermal management schemes. *IEEE Trans. Comp. Pack. Technol.*, **24**, 122–141.

ODDIE, G. & PEARSON, A. J. R. (2004) Flow-rate measurement in two-phase flow. *Annu. Rev. Fluid Mech.*, **36**, 149–172.

ORON, A., DAVIS, S. H. & BANKOFF, S. G. (1997) Long-scale evolution of thin liquid films. *Rev. Mod. Phys.*, **69**, 931–980.

PETTIGREW, K., KIRSHBERG, J., YERKES, K., TREBOTICH, D. & LIEPMANN, D. (2001) Performance of a MEMS based micro capillary pumped loop for chip-level temperature control. *IEEE Instrumentation and Measurement Society, 14th IEEE International Conference on Micro Electro Mechanical Systems*, pp. 427–430.

QU, W. & MUDAWAR, I. (2003) Thermal design methodology for high-heat-flux single-phase and two-phase micro-channel heat sinks. *IEEE Trans. Comp. Pack. Technol.*, **26**, 598–609.

RUSAK, Z. & LEE, J. H. (2004) On the stability of a compressible axisymmetric rotating flow in a pipe. *J. Fluid Mech.*, **501**, 25–42.

SEGIN, T. M. (2004) Nonlinear long-wave interfacial stability of two-layer gas-liquid flows. *Ph.D. Thesis*, New Jersey Institute of Technology.

SEGIN, T. M., TILLEY, B. S. & KONDIC, L. (2004) On undercompressive shocks and flooding in countercurrent two-layer flows. *J. Fluid Mech.*, **532**, 217–242.

STRANG, G. (1988) *Linear Algebra and Its Applications*. New York: Harcourt Brace Jovanovich College Publishers.

TILLEY, B. S., DAVIS, S. H. & BANKOFF, S. G. (1994a) Linear stability theory of two-layer fluid flow in an inclined channel. *Phys. Fluids A*, **6**, 3906–3922.

TILLEY, B. S., DAVIS, S. H. & BANKOFF, S. G. (1994b) Nonlinear long-wave stability of superposed fluids in an inclined channel. *J. Fluid Mech.*, **277**, 55–83.

TREBOTICH, D., KIRSHBERG, J., TENG, J. & LIEPMANN, D. (2001) Optimization of a MEMS based micro capillary pumped loop for chip-level temperature control. *Fourth International Conference on Modeling and Simulation in Microsystems*, pp. 262–265.

YIH, C.-S. (1967) Instability due to viscosity stratification. *J. Fluid Mech.*, **27**, 337–352.

ZHANG, H., MUDAWAR, I. & HASAN, M. M. (2002) Experimental assessment of the effects of body force, surface tension force, and inertia on flow boiling CHF. *Int. J. Heat Mass Transf.*, **45**, 4079–4095.

Appendix A. Derivation of the evolution equation

At O(ε), the $x(\zeta)$-momentum and continuity equations (2.6)–(2.9) yield

$$\mathrm{Re_l}[u_{0\tau}^{(1)} + u_0^{(1)}u_{0\xi}^{(1)} + u_{0\zeta}^{(1)}w_0^{(1)}] = -p_{1\xi}^{(1)} + u_{1\zeta\zeta}^{(1)}, \tag{A.1}$$

$$\mathrm{Re_l}\rho(u_0^{(2)}u_{0\xi}^{(2)} + u_{0\zeta}^{(2)}w_0^{(2)}) = -p_{1\xi}^{(2)} + \mu u_{1\zeta\zeta}^{(2)}, \tag{A.2}$$

$$u_{1\xi}^{(1)} + w_{1\zeta}^{(1)} = 0, \tag{A.3}$$

$$\rho_\tau + (\rho u_1^{(2)})_\xi + (\rho w_1^{(2)})_\zeta = 0, \tag{A.4}$$

$$u_1^{(1)} = 0 \quad (\zeta = 0), \tag{A.5}$$

$$u_1^{(2)} = 0 \quad (\zeta = 1), \tag{A.6}$$

$$w_1^{(1)} = 0 \quad (\zeta = 0), \tag{A.7}$$

$$w_1^{(2)} = 0 \quad (\zeta = 1), \tag{A.8}$$

$$\mu u_{1\zeta}^{(2)} - u_{1\zeta}^{(1)} = 0 \quad (\zeta = h(\xi, \tau)), \tag{A.9}$$

$$w_1^{(2)} - h_\xi u_1^{(2)} - w_0^{(1)} + h_\xi u_0^{(1)} = 0 \quad (\zeta = h(\xi, \tau)). \tag{A.10}$$

Using (A.1)–(A.4) and the boundary and interfacial conditions (A.5)–(A.9), similar to the analysis at the previous order, we arrive at the solution for $u_1^{(i)}$

$$u_1^{(1)} = P_{1\xi}\frac{\zeta^2}{2} + \phi\zeta + F^{(1)}(\xi, \zeta, \tau), \tag{A.11}$$

$$u_1^{(2)} = \tfrac{P_{1\xi}+\alpha}{2\mu}(\zeta - 1)^2 + \psi(\zeta - 1) + F^{(2)}(\xi, \zeta, \tau), \tag{A.12}$$

where

$$\phi = \mu F_\zeta^{(2)}(\xi, h, \tau) - F_\zeta^{(1)}(\xi, h, \tau) - \frac{\mu}{h-1}F^{(2)}(\xi, h, \tau) + \frac{\mu h}{2(h-1)}\{h\sin\beta - p_{0\xi}\} + \alpha\frac{h-1}{2} - P_{1\xi}\frac{h+1}{2}, \tag{A.13}$$

$$\psi = \frac{F^{(2)}(\xi, h, \tau)}{1-h} + \frac{(P_{1\xi}+\alpha)(1-h)}{2\mu} + \frac{h(h\sin\beta - p_{0\xi})}{2(h-1)}, \tag{A.14}$$

$$\alpha = Sh_{\xi\xi\xi} - h_\xi\cos\beta. \tag{A.15}$$

We refer to the Appendix B for the definition of the inertial terms $F^{(i)}$.

Appendix B. Derivation of the inertial terms $F^{(i)}(\xi, \zeta, \tau)$ for compressible case

To find the inertial term $F^{(2)}(\xi, \zeta, \tau)$ in (A.11) and (A.11), we need to solve the problem:

$$F_{\zeta\zeta}^{(2)}(\xi, \zeta, \tau) = \mathrm{Re_l}\frac{\rho}{\mu}(u_0^{(2)}u_{0\xi}^{(2)} + u_{0\zeta}^{(2)}w_0^{(2)}), \tag{B.1}$$

$$F^{(2)}(\xi, 1, \tau) = 0, \tag{B.2}$$

$$F_\zeta^{(2)}(\xi, 1, \tau) = 0. \tag{B.3}$$

After integrating (B.1) and using the boundary conditions (B.2), (B.3), we obtain:

$$F^{(2)}(\xi, \zeta, \tau) = a_1^{(2)}(\zeta - 1)^6 + a_2^{(2)}(\zeta - 1)^5 + a_3^{(2)}(\zeta - 1)^4,$$

$$a_1^{(2)} = \mathrm{Re_l}\frac{\rho p_{0\xi}}{120\mu^3}\left(\frac{h_\xi p_{0\xi}}{1-h} - \frac{\rho_\xi}{\rho}p_{0\xi}\right),$$

$$a_2^{(2)} = \mathrm{Re_l}\frac{\rho p_{0\xi}}{80\mu^3}(1-h)\left(\frac{h_\xi p_{0\xi}}{1-h} - \frac{\rho_\xi}{\rho}p_{0\xi}\right),$$

$$a_3^{(2)} = \mathrm{Re_l}\frac{\rho p_{0\xi}}{48\mu^3}(1-h)^2\left(\frac{h_\xi p_{0\xi}}{1-h} - \frac{\rho_\xi}{\rho}p_{0\xi}\right).$$

Similarly for $F^{(1)}(\xi, \zeta, \tau)$ we have:

$$F^{(1)}_{\zeta\zeta}(\xi, \zeta, \tau) = \mathrm{Re_l}[u^{(1)}_{0\tau} + u^{(1)}_0 u^{(1)}_{0\xi} + u^{(1)}_{0\zeta} w^{(1)}_0], \tag{B.4}$$

with the following boundary conditions:

$$F^{(1)}(\xi, 0, \tau) = 0, \tag{B.5}$$

$$F^{(1)}_{\zeta}(\xi, 0, \tau) = 0. \tag{B.6}$$

After integrating (B.4) and applying the boundary conditions (B.5), (B.6):

$$F^{(1)}(\xi, \zeta, \tau) = a^{(1)}_1 \zeta^6 + a^{(1)}_2 \zeta^5 + a^{(1)}_3 \zeta^4 + a^{(1)}_4 \zeta^3, \tag{B.7}$$

where

$$a^{(1)}_1 = \mathrm{Re_l} \frac{p_{0\xi\xi\xi}}{360}(p_{0\xi} - \sin\beta),$$

$$a^{(1)}_2 = \mathrm{Re_l} \frac{p_{0\xi\xi\xi}}{60}\left\{h\sin\beta - \frac{p_{0\xi}}{2}(h+1)\right\},$$

$$a^{(1)}_3 = \mathrm{Re_l} \frac{1}{24}\left\{p_{0\xi\tau} + \left[h\sin\beta - \frac{p_{0\xi}}{2}(h+1)\right]\left[h_\xi \sin\beta - \frac{p_{0\xi\xi\xi}}{2}(h+1) - \frac{p_{0\xi} h_\xi}{2}\right]\right\},$$

$$a^{(1)}_4 = \mathrm{Re_l} \frac{2h_\tau \sin\beta - p_{0\xi\tau}(h+1) - h_\tau p_{0\xi}}{12}.$$

Appendix C. Definition of the coefficients in the system of characteristic equations

The coefficients entering the system of characteristic equations (3.14)–(3.15) are as follows:

$$\bar{b}_1 = b_1 + \varepsilon \mathrm{Re_l}\theta_6, \quad \bar{b}_2 = b_2 + \varepsilon \mathrm{Re_l}\theta_1, \quad \bar{b}_3 = b_3 + \varepsilon \mathrm{Re_l}\theta_2,$$
$$\bar{b}_4 = b_4 + \varepsilon \mathrm{Re_l}\theta_3, \quad \bar{b}_6 = \varepsilon \mathrm{Re_l}\theta_4, \quad \bar{b}_7 = \varepsilon \mathrm{Re_l}\theta_5,$$
$$\bar{a}_1 = a_1 + \mathrm{Re_l}\gamma_3, \quad \bar{a}_2 = a_2 + \mathrm{Re_l}\gamma_1, \quad \bar{a}_3 = a_3 + \mathrm{Re_l}\gamma_4,$$
$$\bar{a}_4 = a_4 + \mathrm{Re_l}\gamma_5, \quad \bar{a}_5 = a_5 + \mathrm{Re_l}\gamma_6, \quad \bar{a}_6 = \mathrm{Re_l}\gamma_2, \quad \alpha = \frac{D}{240} h_0^4 (7h_0 + 25),$$

with

$$a_1 = \frac{D}{12}\frac{-h_0^2 + 2h_0 + 3}{(1-h_0)^2}(\rho^2_{0\xi} + 2\varepsilon\rho_{0\xi}\rho_{1\xi}) + \frac{D(1-h_0)}{6\varepsilon\mu}[\rho^2_{0\xi} + \rho_0\rho_{0\xi\xi} + \varepsilon(\rho_0\rho_1)_{\xi\xi}],$$

$$a_2 = -\frac{D}{4}\left(\frac{1+h_0}{1-h_0}\right)^2(\rho_0\rho_{0\xi} + \varepsilon(\rho_0\rho_1)_\xi) + \frac{h_0(h_0+2)}{4(1-h_0)}(\rho_0 + \varepsilon\rho_1)\sin\beta$$
$$+ \frac{D}{4\varepsilon\mu}(1-h_0)(\rho_0\rho_{0\xi} + \varepsilon(\rho_0\rho_1)_\xi),$$

$$a_3 = -\frac{D}{12\varepsilon\mu}(1-h_0)^2(\rho_{0\xi\xi} + \varepsilon\rho_{1\xi\xi}),$$

$$a_4 = \frac{h_0^2}{4}\sin\beta + \frac{D}{6}\frac{h_0^2(h_0+3)}{1-h_0}(\rho_{0\xi}+\varepsilon\rho_{1\xi}) - \frac{D(1-h_0)^2}{6\varepsilon\mu}(\rho_{0\xi}+\varepsilon\rho_{1\xi}),$$

$$a_5 = -\frac{D(1-h_0)^2}{12\varepsilon\mu}(\rho_0+\varepsilon\rho_1), \quad b_1 = -\frac{D}{12}h_0^2(h_0+3) + \varepsilon\frac{\mu D h_0^3}{4(1-h_0)},$$

$$b_2 = \frac{D}{4}h_0(h_0+2)(\rho_{0\xi\xi}+\varepsilon\rho_{1\xi\xi}) + \frac{\varepsilon\mu D}{4}\left[\frac{h_0^3\rho_{0\xi\xi\xi}}{(1-h_0)^2} + \frac{3h_0^2}{1-h_0}\rho_{0\xi\xi}\right],$$

$$b_3 = h_0^2\sin\beta - \frac{D}{4}h_0(h_0+2)(\rho_{0\xi}+\varepsilon\rho_{1\xi}) - \frac{\varepsilon\mu}{4}\sin\beta\frac{h_0^3(4-3h_0)}{(1-h_0)^2} + \frac{\varepsilon\mu D}{4}\frac{h_0^2(3-2h_0)}{(1-h_0)^2}\rho_{0\xi},$$

$$b_4 = -\varepsilon\frac{h_0^3}{3}\cos\beta, \quad b_5 = \varepsilon\frac{S}{3}h_0^3,$$

and

$$\theta_1 = -\frac{D^2}{20160}\left[\frac{3\rho_{0\xi}^2\rho_{0\xi\xi\xi}}{\rho_0} - \frac{\rho_{0\xi}^4}{\rho_0^2}\right]h_0^4(203h_0^2+966h_0-1890) + \frac{13}{240}\frac{D^2}{\mu^2}\rho_0\rho_{0\xi}\rho_{0\xi\xi}h_0(2-7h_0)(1-h_0)^4 + \frac{D}{10080}\sin\beta h_0^5(763h_0+882)\left[\frac{2\rho_{0\xi}\rho_{0\xi\xi}}{\rho_0} - \frac{\rho_{0\xi}^3}{\rho_0^2}\right],$$

$$\theta_2 = -\frac{D^2}{1680}\frac{h_0^5(10h_0^2+7h_0+77)}{1-h_0}\rho_{0\xi}\rho_{0\xi\xi} - \frac{D^2}{20160}\frac{\rho_{0\xi}^3}{\rho_0}h_0^4(203h_0^2+966h_0-1890) - \frac{13}{480}\frac{D^2}{\mu^2}h_0^2(1-h_0)^4[\rho_{0\xi}^3+2\rho_0\rho_{0\xi}\rho_{0\xi\xi}] + \frac{13}{480}\frac{D^2}{\mu^2}h_0(1-h_0)^4(2-7h_0)\rho_0\rho_{0\xi}^2 + \sin\beta\left[\frac{D}{840}\frac{h_0^5(41h_0^2-49h_0-56)}{1-h_0}\rho_{0\xi\xi} + \frac{D}{1440}\frac{\rho_{0\xi}^2}{\rho_0}h_0^5(109h_0+126)\right],$$

$$\theta_3 = -\frac{D^2}{3360}\frac{h_0^5(10h_0^2+7h_0+77)}{1-h_0}\rho_{0\xi}^2 + \frac{2}{15}h_0^6\sin^2\beta - \frac{13}{480}\frac{D^2}{\mu^2}\rho_0\rho_{0\xi}^2h_0^2(1-h_0)^4 + \frac{D}{840}\sin\beta\frac{h_0^5(41h_0^2-49h_0-56)}{1-h_0}\rho_{0\xi},$$

$$\theta_4 = -\frac{D^2}{20160}\left[\frac{2\rho_{0\xi}^4}{\rho_0^3} - \frac{3\rho_{0\xi}^2\rho_{0\xi\xi}}{\rho_0^2}\right]h_0^5(29h_0^2+161h_0-378) + \frac{13}{240}\frac{D^2}{\mu^2}\rho_{0\xi}\rho_{0\xi\xi}h_0^2(1-h_0)^5 + \frac{D}{5040}\sin\beta h_0^6(109h_0+147)\left[\frac{\rho_{0\xi}^3}{\rho_0^3} - \frac{\rho_{0\xi}\rho_{0\xi\xi}}{\rho_0^2}\right],$$

$$\theta_5 = -\frac{D^2}{10080}\left[\frac{3\rho_{0\xi}\rho_{0\xi\xi}}{\rho_0} - \frac{2\rho_{0\xi}}{\rho_0}\right]h_0^5(29h_0^2 + 161h_0 - 378)$$
$$+ \frac{13}{240}\frac{D^2}{\mu^2}\rho_0\rho_{0\xi\xi}h_0^2(1-h_0)^5 + \frac{D}{10080}\sin\beta h_0^6(109h_0 + 147)\left[\frac{2\rho_{0\xi\xi}}{\rho_0} - \frac{3\rho_{0\xi}^2}{\rho_0^2}\right],$$
$$\theta_6 = -\frac{D^2}{6720}\frac{\rho_{0\xi}^2}{\rho_0}h_0^5(29h_0^2 + 161h_0 - 378) + \frac{13}{240}\frac{D^2}{\mu^2}\rho_0\rho_{0\xi}h_0^2(1-h_0)^5$$
$$+ \frac{D}{5040}\sin\beta h_0^6(109h_0 + 147)\frac{\rho_{0\xi}}{\rho_0},$$

and

$$\gamma_1 = -\frac{51}{1120\mu^3}(1-h_0)^5(\rho_0\rho_{0\xi}^3 + \varepsilon[\rho_1\rho_{0\xi}^3 + 3\rho_0\rho_{0\xi}^2\rho_{1\xi}])$$
$$-\frac{17}{1680\mu^3}(1-h_0)^5(\rho_0^2\rho_{0\xi}\rho_{0\xi\xi} + \varepsilon\rho_0[\rho_0\rho_{0\xi\xi}\rho_{1\xi} + \rho_0\rho_{0\xi}\rho_{1\xi\xi} - 2\rho_{0\xi}\rho_{0\xi\xi}\rho_1]),$$
$$\gamma_2 = -\frac{17}{3360\mu^3}(\rho_0^2\rho_{0\xi}^2 + 2\varepsilon\rho_0\rho_{0\xi}^2(\rho_0\rho_1)_\xi)(1-h_0)^5,$$
$$\gamma_3 = \frac{17}{560\mu^3}(\rho_{0\xi}^4 + 4\varepsilon\rho_{0\xi}^3\rho_{1\xi})(1-h_0)^5$$
$$-\frac{51}{560\mu^3}(1-h_0)^5(\rho_0\rho_{0\xi}^2\rho_{0\xi\xi} + \varepsilon\rho_{0\xi}[2\rho_0\rho_{0\xi\xi}\rho_{1\xi} + \rho_{0\xi}\rho_{0\xi\xi}\rho_1 + \rho_0\rho_{0\xi}\rho_{1\xi\xi}]),$$
$$\gamma_4 = \frac{17}{1120\mu^3}(\rho_{0\xi}^2\rho_{0\xi\xi} + \varepsilon\rho_{0\xi}[\rho_{0\xi}\rho_{1\xi\xi} + 2\rho_{0\xi\xi}\rho_{1\xi}])(1-h_0)^6,$$
$$\gamma_5 = \frac{17}{840\mu^3}(1-h_0)^6(\rho_{0\xi}^3 + 3\varepsilon\rho_{0\xi}^2\rho_{1\xi})$$
$$+\frac{17}{560\mu^3}(1-h_0)^6(\rho_0\rho_{0\xi}\rho_{0\xi\xi} + \varepsilon[\rho_0\rho_{0\xi\xi}\rho_{1\xi} + \rho_1\rho_{0\xi}\rho_{0\xi\xi} + \rho_0\rho_{0\xi}\rho_{1\xi\xi}]),$$
$$\gamma_6 = \frac{17}{1120\mu^3}(1-h_0)^6(\rho_0\rho_{0\xi}^2 + \varepsilon\rho_{0\xi}[2\rho_0\rho_{1\xi} + \rho_{0\xi}\rho_1]).$$